Bulletin of Earthquake Engineering (2020) 18:1187–1212
https://doi.org/10.1007/s10518-019-00748-4

ORIGINAL RESEARCH

Effects of soil-foundation-structure interaction on fundamental frequency and radiation damping ratio of historical masonry building sub-structures

Annachiara Piro[1] · Filomena de Silva[2] · Fulvio Parisi[1] · Anna Scotto di Santolo[3] · Francesco Silvestri[2]

Received: 7 May 2019 / Accepted: 30 October 2019 / Published online: 5 November 2019

Abstract
Large-scale simulations and forensic analyses of the seismic behaviour of real case studies are often based on simplified analytical approaches to estimate the reduction in fundamental frequency and the amount of radiation damping induced by dynamic soil-foundation-structure (SFS) interaction. The accuracy of existing closed-form solutions may be limited because they were derived through single degree-of-freedom structural models with shallow rigid foundations placed on a homogeneous, linear elastic half-space. This paper investigates the effectiveness of those formulations in capturing the dynamic out-of-plane response of single load-bearing walls within unreinforced masonry buildings having either a shallow foundation or an underground storey embedded in layered soil. To that aim, analytical predictions based on the replacement oscillator approach are compared to results of two-dimensional dynamic analyses of coupled SFS elastic models under varying geotechnical and structural properties such as the soil stratigraphy, foundation depth and number of building storeys. Regression models and a relative soil-structure stiffness parameter are proposed to quickly predict the frequency reduction induced by SFS interaction, accounting for the presence of an embedded foundation, an underground storey and a layered soil. The effects of SFS interaction are also evaluated in terms of equivalent damping ratio, showing the limitations of simplified approaches. Since the geometric layouts considered in this study are rather recurrent in the Italian and European built heritage, the proposed procedure can be extended to similar structural configurations.

Keywords Soil-structure interaction · Historical masonry buildings · Time history analysis · Regression models · Equivalent damping ratio · Fundamental frequency of vibration

✉ Annachiara Piro
annachiara.piro@unina.it

Extended author information available on the last page of the article

1 Introduction

Fixed-base capacity models are commonly adopted in seismic assessment of building structures. However, structural response can be strongly influenced by dynamic interaction with underlying soil (Mylonakis and Gazetas 2000; Kausel 2010). Soil-structure interaction (SSI) can produce a reduction in the fundamental frequency of the soil-foundation-structure (SFS) system as well as additional energy dissipation by means of wave radiation and hysteresis of soil (Gazetas 1983; Wolf 1985; Mylonakis et al. 2006; Givens et al. 2016). These SSI effects can be associated with the soil compliance to the structural motion, which is usually referred to as inertial interaction. This type of interaction produces the aforementioned modification of the period and damping of the whole system, affecting the structural response in terms of displacements and/or accelerations. As the foundation embedment increases, another SSI effect due to the relative soil-foundation stiffness is observed and is referred to as kinematic interaction (Elsabee and Morray 1977; Kim and Stewart 2003). This consists of a modification of seismic motion transmitted from the soil to the structure with respect to free-field conditions. In this respect, analytical solutions for continuum models (Beredugo and Novak 1972; Meek and Wolf 1994; Jaya and Meher Prasad 2002) and multi-spring models (Gerolymos and Gazetas 2006a, b, c; Karapiperis and Gerolymos 2014), as well as numerical results of boundary and finite element models (Kausel and Roesset 1975; Dominguez 1978; Spyrakos and Beskos 1986; Varun et al. 2009; Conti et al. 2016; Jahankhah and Farashahi 2017), have been proposed to quantify modifications in the seismic signal crossing stiff and embedded foundations.

Another important SSI effect occurs under strong motions, when the foundation swaying and rocking induce cyclic high strain levels in the surrounding soil until its yielding. This failure of the foundation soil contributes to the dissipation of seismic energy, causing a reduction in displacement demand on structures (Faccioli et al. 1998; Shirato et al. 2008; Gazetas 2015). This has a beneficial effect on seismic performance of structures, particularly in the case of masonry buildings that typically have low displacement capacity compared to other types of constructions [see experimental studies by, amongst others, Tomaževič and Weiss (2010), Augenti et al. (2011) and Kallioras et al. (2018)]. In addition, displacement capacity is a structural feature that is rather difficult to be increased without compromising the artistic value of a historical construction. Recent guidelines and studies on seismic performance assessment of historical masonry buildings (Lagomarsino and Cattari 2015; Guerrini et al. 2017) have thus pointed out the importance of displacement-based approaches, keeping in mind that these constructions suffer cracking even under low-intensity earthquakes so their survivability strongly depends on acceptable levels of displacement capacity.

In order to account for inertial interaction effects in seismic performance assessment, more or less refined models of soil and structure have been proposed. The use of either finite element or finite difference models is generally adopted for single case studies (Casciati and Borja 2004; Pitilakis and Karatzetzou 2015; de Silva et al. 2018; Cattari et al. 2019) because of their huge computational demand. The simplest model of a SFS system is the replacement oscillator (RO) in which the structure is reduced to a single degree-of-freedom (SDOF) system (Veletsos and Meek 1974). The RO is equipped at the base with a combination of linear springs, which are associated with translational and rotational motion, plus as many viscous dashpots simulating the impedance of a homogeneous, linear elastic half-space underlying a circular rigid foundation at the ground surface (Veletsos and Nair 1975; Veletsos and Meek 1974) or embedded in the soil (Bielak 1975; Stewart et al.

1999). Some applications of the simplified approach were made by Madiai et al. (2013), Ceroni et al. (2014) and Cosentini et al. (2015). The sensitivity of inertial interaction to the foundation depth has been mostly investigated by modifying the stiffness of springs and damping coefficients (Gazetas 1991; Aviles and Perez-Rocha 1996, 1998; de Silva et al. 2018). Equivalent properties are required to consider the flexibility (Pitilakis and Karatzetzou 2015) and complex geometry of foundations, as well as the presence of a layered soil (Gazetas 1983; Stewart et al. 2003). This aspect is a significant limitation in seismic performance assessment of historical masonry buildings, which are frequently characterised by irregular underground storeys or foundations embedded in layered soil. Recently, the authors investigated some case studies of historical buildings (Piro et al. 2018; Vuoto et al. 2018), demonstrating that the presence of an underground floor can influence the dynamic behaviour and repairability of the SFS system, the latter feature measured in terms of residual-to-maximum drift ratio of masonry walls (see e.g. Parisi et al. 2014).

In this study, two-dimensional (2D) SFS systems derived from case-study buildings in Vuoto et al. (2018) were analysed to assess the seismic performance of out-of-plane (OOP) loaded masonry walls. This was motivated by the fact that OOP failure modes are usually observed during post-earthquake damage inspections (de Silva et al. 2016; Bruneau 1994; Augenti and Parisi 2010a; D'Ayala and Paganoni 2011; Penna et al. 2014; Sorrentino et al. 2014).

The aim of this research was threefold: (i) to evaluate the effects of underground storeys and layered soil on dynamic behaviour, fundamental frequency and damping ratio of SFS systems that consider OOP loaded masonry walls in elevation; (ii) to calibrate RO properties for the estimation of the elastic seismic demand in simplified performance assessment of masonry walls against local failure modes, particularly in terms of their potential activation; and (iii) to propose a relative soil-structure stiffness parameter that allows one to identify whether SSI should be considered and, in such a case, to estimate the expected value of natural frequency of the SFS system. Since this study is based on the assumption of soil and structural properties associated with very low strain levels, the methodology and its results in terms of frequency and damping ratio can also be used to integrate the output of structural health monitoring under ambient noise vibrations. Even though 2D models that represent transverse sections of historical masonry buildings were considered, the analysis procedure and results presented herein can be applied to several kinds of constructions located in the Euro-Mediterranean region (Augenti and Parisi 2019).

2 Methodology

This research makes use of two modelling approaches: the former is explicitly based on coupled SFS systems, whereas the latter relies upon replacement oscillators. In the first stage of this study, 2D finite difference dynamic models corresponding to realistic patterns of soil and masonry structure with underground storey were developed. A series of parametric analyses were carried out varying geotechnical and structural properties, including the type and depth of building basement (i.e. embedded foundation or underground storey), soil layering (i.e. homogeneous or layered soil, the latter with different combinations of material properties), and number of building storeys. Thereafter the results of the sensitivity analysis were used to calibrate RO properties in complex conditions that are different from those assumed in the original formulation by Veletsos and Meek (1974). Indeed, those researchers assumed that the seismic response of a SFS system depends on four factors, namely: the relative soil-structure stiffness and relative soil-structure mass inertia, which are associated with soil and structural properties; the slenderness of the structure; the ratio of the input motion frequency to the natural frequency of the fixed-base structure. In this study, a modification of the abovementioned relative soil-structure stiffness parameter is proposed to estimate the fundamental frequency by taking into account a layered soil and a foundation system composed by either an embedded "floating" shallow foundation or an underground floor.

2.1 SFS interaction models

SFS systems were developed in FLAC 2D ver. 7.0 (Itasca 2011) according to the finite difference (FD) method. Two subsoil configurations were distinctly considered and associated with code-conforming ground types, namely, homogeneous and layered soil, the latter consisting of two layers with thickness denoted as shallow cover t_1 and in-depth formation t_2.

Two configurations of building basements were also adopted, as follows:

(i) embedded "floating" foundation with depth $D < t_1$ (Fig. 1a);
(ii) underground storey with bearing wall foundation, reaching a depth $D = t_1$ (Fig. 1b).

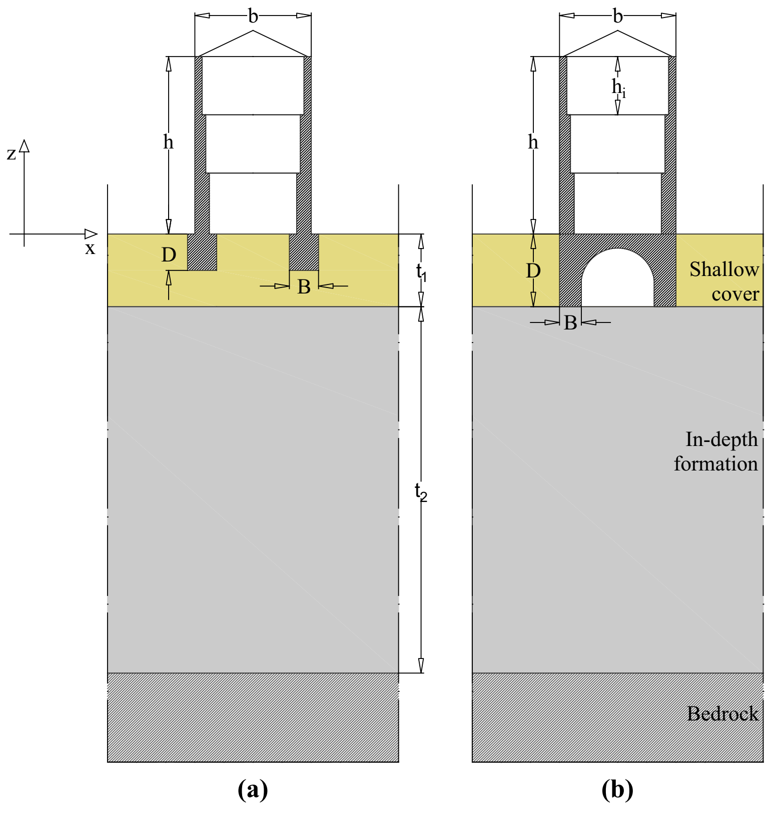

Fig. 1 SFS models with different configurations of basement: **a** embedded floating foundation; **b** underground storey with bearing wall foundation

The seismic bedrock was simulated through an additional layer with finite thickness, which was placed below the in-depth formation and characterised by the properties of ground type A according to Eurocode 8 (EC8) (CEN 2004) and Italian Building Code (MIT 2018). Interface elements were not used because very low strain levels were mobilised during the analyses under random noise. Consequently, separations or slippage between the soil and foundation were not expected to occur.

Regardless of the basement and soil configuration, the structural system was regarded as transverse section of an unreinforced masonry building. The elevation of each masonry structure consisted of two slender load-bearing walls that were connected each other by single-span floor systems and a pitched roof. The thickness of the walls was reduced along the building height, leading to a fairly homogeneous distribution of vertical stresses from the ground floor to the top.

By contrast, inter-storey height was assumed to be constant along the building elevation. Floor and roof systems were modelled through one-dimensional (1D) beam elements with pinned connections to load-bearing walls. Each structural model was assumed to have variable height h and constant width b, whereas a fixed depth of 30 m, which is equal to t_1+t_2 in Fig. 1, was assigned to the bedrock. As observed in many historical buildings (Augenti and Parisi 2019), shallow foundations were assumed to be made of the same masonry type of the structure in elevation. The inertia mass of the structure was defined by the size and mass density of masonry walls and floor elements. The inertia mass of the roof was incorporated in that of the upper floor element.

Being the parametric study addressed to examine SSI effects well below structural and geotechnical failure states, FD models of soil, foundation and structure were analysed by assuming a linear elastic behaviour of materials. Accordingly, the damping ratios of the soil and structural materials (respectively denoted as ξ_{soil} and ξ_{str} below) were set to 0.1%, assuming very low strain levels under low-amplitude excitations. The soil was modelled as a medium with variable sets of values for shear wave velocity V_S, mass density ρ, shear modulus G and Poisson's ratio ν. Constant properties were used for the floors and the masonry, this latter regarded as an equivalent homogeneous material according to the macro-modelling approach (Lourenço 1996). Such hypothesis allows for assessing the macroscopic behaviour of masonry components (i.e. walls and foundations), overlooking a detailed description of local stress/strain fields within individual masonry constituents (i.e. bricks/stones and mortar joints). The macro-modelling approach significantly reduces the computational cost and was successfully validated for a number of historical masonry types (see e.g. Parisi et al. 2019).

2.2 Equivalent parameters of the replacement oscillators

The analytical approach followed in this study derives from the interpretation of the dynamic behaviour of the so-called replacement oscillator (RO), which is a simplified dynamic system proposed by Veletsos and Meek (1974). The latter is a fixed-base SDOF system with equivalent mass m^*, lateral stiffness k^* and damping ratio ξ^* (Fig. 2d), properly calibrated to achieve the same dynamic behaviour of a compliant-base SDOF system supported by translational and rotational springs and dashpots (Fig. 2c). The equivalent mass, m^*, is typically set equal to the inertia mass of the above-ground structure involved in the dynamic motion (i.e. $m^*=m_{str}$). In this study, the mass m_{str} was assumed as the effective inertia mass corresponding to the fundamental mode of vibration of the fixed-base structure, as follows:

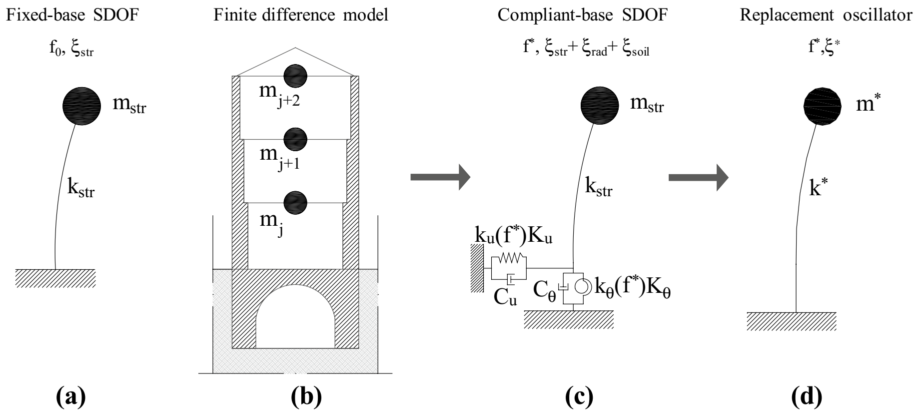

Fig. 2 Definition of replacement oscillator of SFS system

$$m_{str} = \sum_{j=1}^{n} m_j \phi_j \tag{1}$$

where j denotes a floor level; n is the number of floor levels; m_j is the inertia mass of the j-th floor level; and ϕ_j is the first-mode displacement of the j-th floor level.

The equivalent stiffness, k^*, takes into account the fixed-base stiffness of the structure, k_{str}, and that of the translational and rotational base springs expressed by the corresponding impedance functions $\bar{K}_u$ and $\bar{K}_\theta$.

The fundamental modal shape of the fixed-base structure (Fig. 2b) was computed through dynamic analysis of the SFS system with firm soil (i.e. soil type A) under a noise input signal. The same time history analysis allowed for evaluating the fundamental frequency of the fixed-base system, f_0, so that the stiffness of an equivalent fixed-base SDOF (Fig. 2a) could be computed as follows:

$$k_{str} = 4\pi^2 f_0^2 m_{str} \tag{2}$$

The equivalent damping ratio, ξ^*, is assumed to be the sum of structural damping, radiation damping and soil damping, i.e. $\xi^* = \xi_{str} + \xi_{rad} + \xi_{soil}$. In this study, soil material damping, ξ_{soil}, was not considered in accordance to the approach proposed by Veletsos and Meek (1974), which was implemented to calculate the fundamental period and equivalent damping ratio of the oscillators replacing the SFS systems described in Sect. 2.1. Moreover, this study investigates the SFS interaction under very low strain levels, where ξ_{soil} is generally negligible. The structural damping, ξ_{str}, was assumed as low as 0.1% to directly quantify the radiation damping of the SFS system in the replacement oscillator model.

The foundation impedance functions $\bar{K}_u$ and $\bar{K}_\theta$ assigned to the base of the SDOF model were calculated according to the formulas proposed by Gazetas (1991):

$$\bar{K}_u = k_u(f^*)K_u + i\,2\pi f^* c_u(f^*)C_u \tag{3}$$

$$\bar{K}_\theta = k_\theta(f^*)K_\theta + i\,2\pi f^* c_\theta(f^*)C_\theta \tag{4}$$

where i is the imaginary unity; f^* is the fundamental frequency of the RO system; $k_u(f^*)$ and $k_\theta(f^*)$ are translational and rotational dynamic stiffness coefficients; K_u and K_θ are translational and rotational components of the foundation static stiffness; $c_u(f^*)$ and $c_\theta(f^*)$

are the dynamic damping coefficients; C_u and C_θ are damping coefficients, accounting for the energy dissipated by waves spreading from the foundation (radiation damping) and soil hysteresis (material damping). The latter contribution to damping was neglected in this study.

The translational and rotational components of static stiffness, as well as the radiation damping coefficients, were defined by Gazetas (1991) as functions of the following properties: shear modulus G and Poisson's ratio ν of the soil; length L, width B and depth D of the foundation; and a dimensionless frequency parameter defined as follows:

$$a_0 = \frac{2\pi f^* B}{V_S} \tag{5}$$

The fundamental frequency of the RO (equal to that of the flexible-base SDOF system) was calculated in accordance to Veletsos and Meek (1974) by means of the following equation:

$$\frac{f_0}{f^*} = \sqrt{1 + \frac{k_{str}}{\mathrm{Re}\left(\bar{K}_u\right)}\left(1 + \frac{\mathrm{Re}\left(\bar{K}_u\right)}{\mathrm{Re}\left(\bar{K}_\theta\right)}\frac{h^2}{r^2}\right)} \tag{6}$$

where h is the height of the structure (Fig. 1); $\mathrm{Re}\left(\bar{K}_u\right) = k_u(f^*)K_u$ is the real part of translational impedance function into Eq. (3); and $\mathrm{Re}\left(\bar{K}_\theta\right) = k_\theta(f^*)K_\theta$ is the real part of rotational impedance function into Eq. (4). For each soil-foundation system, the impedance functions were calculated through Eqs. (3) and (4), following an iterative procedure so that the difference between the frequency computed via Eq. (6) and that associated with a_0 was equal to zero.

After that the frequency of the SFS system was obtained, the equivalent damping was first computed as follows (Veletsos and Meek 1974):

$$\xi^* = \left(\frac{f^*}{f_0}\right)^3\left[\xi_{str} + \frac{(2-\nu)\pi^4\mu}{2\sigma^3}\left(\frac{c_u(f^*)}{k_u(f^*)^2}\frac{r^2}{h^2} + \frac{c_\theta(f^*)}{k_\theta(f^*)^2}\right)\right] \tag{7}$$

where r is the radius of a circle with the same area of the actual foundation; σ is the relative soil-structure stiffness parameter defined as follows:

$$\sigma = \frac{V_S}{f_0\, h} \tag{8}$$

μ is the relative mass density for the structure and soil, which is defined as follows:

$$\mu = \frac{m_{str}}{\rho\pi r^2 h} \tag{9}$$

The computation of frequency and damping ratio of the SFS systems was repeated following the more recent approach proposed by Maravas et al. (2014). The equivalent damping ratio was thus computed as follows:

$$\xi^* = S\left[\frac{\xi_u}{\omega_u^2\left(1+4\xi_u^2\right)} + \frac{\xi_\theta}{\omega_\theta^2\left(1+4\xi_\theta^2\right)} + \frac{\xi_{str}}{\omega_0^2\left(1+4\xi_{str}^2\right)}\right] \tag{10}$$

where ξ_u and ξ_θ are energy loss coefficients that are similar to viscous damping ratios and equal to the ratio between the imaginary and real part of the impedance functions; ξ_{str} is the structural damping; ω_u, ω_θ and ω_0 are the uncoupled circular natural frequencies of the system, respectively under swaying oscillation of the base, rocking oscillation and oscillation of the fixed-base structure; S is a factor defined by Eq. (11) and is used to calculate the fundamental frequency f^* through Eq. (12).

$$S = \left[\frac{1}{\omega_u^2\left(1 + 4\xi_u^2\right)} + \frac{1}{\omega_\theta^2\left(1 + 4\xi_\theta^2\right)} + \frac{1}{\omega_0^2\left(1 + 4\xi_{str}^2\right)} \right]^{-1} \tag{11}$$

$$f^{*2} = \frac{S}{4\pi^2\left(1 + 4\xi^{*2}\right)} \tag{12}$$

2.3 Definition of relative soil-structure stiffness parameter

Considering a linear visco-elastic SDOF system with rigid foundation placed on ground surface of a homogeneous half-space, Veletsos and Meek (1974) proposed diagrams that show variations of fundamental frequency and damping ratio as functions of the relative soil-structure stiffness parameter, σ. Those diagrams can be used for a quick estimation of SSI effects, but they cannot be directly applied to the cases of this study in which a layered soil and structures with embedded foundation and/or underground storey are considered. To this aim, an equivalent soil-structure stiffness parameter, σ_{eq}, was defined by properly modifying the shear wave velocity, while keeping h as height of the above-ground structure and f_0 as fixed-base frequency. Such a modified velocity is herein defined as equivalent shear wave velocity and is denoted by $V_{S,eq}$. This parameter was computed in the soil volume expected to be excited by the foundation motion. Such a volume was assumed to have depth and surface width equal to twice the building width b, which is compatible with the soil volume usually affected by the presence of a structure. In the following, numerical results will be expressed as a function of either the proposed parameter σ_{eq} or the classical parameter σ, the latter depending only on the shear wave velocity of the upper soil layer. It is worth noting that Gazetas (1983) and Stewart et al. (2003) suggested that the soil affected by the foundation swaying and rocking extends to a depth less than half the foundation width, which is almost coincident with the depth of the upper soil layer for the analysed case studies. Nevertheless, although the depth of the effective soil volume is typically set to $b/2$ in the computation of impedance functions, there is no general consensus on the soil volume mobilised during earthquake excitation because of the huge variability in the structural response. As shown in Fig. 3, the aforementioned volume includes fractions of the top and bottom soil layers, the structure and the void space of the underground storey. Such components of the SFS system can be respectively numbered as 1, 2, 3 and 4, so that an equivalent shear modulus G_{eq} and an equivalent mass density ρ_{eq} can be defined through the following equations:

$$G_{eq} = \frac{\sum_{j=1}^{4} \alpha_j G_j A_j}{\sum_{j=1}^{4} A_j} \tag{13}$$

$$\rho_{eq} = \frac{\sum_{j=1}^{4} \alpha_j \rho_j A_j}{\sum_{j=1}^{4} A_j} \tag{14}$$

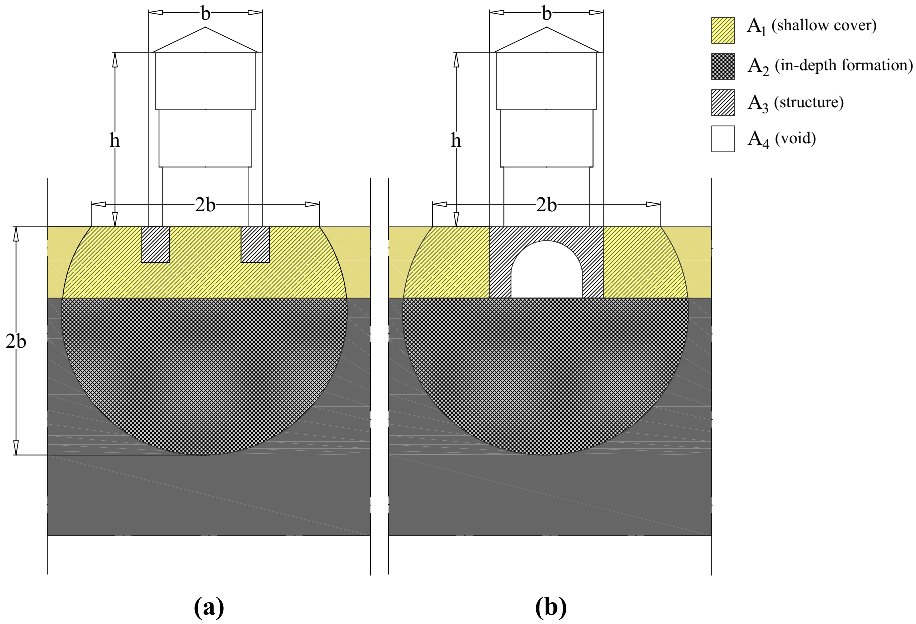

Fig. 3 Soil volume affected by horizontal foundation motion: **a** embedded floating foundation; **b** underground storey with bearing wall foundation

where G_j, ρ_j, A_j and α_j respectively stand for the shear modulus, mass density, area and weighting coefficient of the j-th part of the SFS system ($j = 1,\ldots,4$). In case of homogeneous soil, G_1 and G_2 turn out to be equal.

Thus, the equivalent shear wave velocity of the SFS system can be computed as follows:

$$V_{S,eq} = \sqrt{\frac{G_{eq}}{\rho_{eq}}} \tag{15}$$

The weighting coefficients α_j need to be numerically calibrated (see Sect. 4) because they depend on the ratios between properties of the SFS system. In this way, the same extension of the soil volume can be used for different soil-foundation configurations, since the relevance of each component in the different SFS systems is governed by the variability of the weighting coefficients.

3 Description of case studies

SFS systems and their equivalent oscillators were generated by assuming alternative configurations of building basement (i.e. embedded floating foundation or underground storey) and soil (i.e. homogeneous or layered), as well as three variants of tuff stone masonry structure with different number of storeys (i.e. 2, 3 or 4). Four types of soil, denoted as A, B, C and D as in EC8 (CEN 2004), were alternatively assigned to homogeneous subsoil models. Three combinations of shallow cover and in-depth formation were assumed in the case of layered soil, namely C-B, D-B and D-C. Preliminary analyses allowed the authors to remove other combinations of soil layers that did not produce significant SSI effects on the building sub-structures considered in this study. Therefore, a total of 42 case studies were assumed. A multi-parametric analysis was carried out by keeping constant the following properties:

(i) thickness of shallow cover and in-depth formation, which was assumed equal to $t_1 = 5$ m and $t_2 = 25$ m, respectively;
(ii) width and inter-storey height of the building, which were respectively set to $b = 8$ m and $h_i = 4$ m according to typical sizes detected in historical buildings (see e.g. Augenti and Parisi 2019);
(iii) mass density and Poisson's ratio of structural materials, i.e. masonry and homogenised (ideal) material of floor- and roof-equivalent beam elements.

The depth of the embedded foundation was set to $D = 2.5$ m, whereas the height of the underground storey was set to $D = t_1 = 5$ m. According to the inter-storey height considered, the structural systems with 2, 3 and 4 storeys above ground had aspect ratios h/b equal to 1, 1.5 and 2, respectively. The subsoil domain was assumed to have a width of 50 m and bedrock depth of 30 m. The top of the bedrock was included in the domain through a finite layer with thickness of 5 m. The infinite extension of bedrock in depth was simulated by dashpots attached to the bottom nodes, oriented along the normal and shear directions. Consequently, the input motion (Fig. 5) was applied as shear stress time history (see Sect. 4). To minimize the model size, free-field boundary conditions were imposed along the vertical sides of soil volume, simulating an ideal horizontally layered soil profile connected to the main-grid domain through viscous dashpots. The soil was discretised into a mesh of quadrilateral elements, the size of which was defined by satisfying the criterion by Kuhlemeyer and Lysmer (1973) for accurate modelling of shear wave propagation up to frequencies of 25 Hz.

Figure 4 shows the FD models that were developed for the case-study SFS systems by considering homogeneous (Fig. 4a, b) and layered (Fig. 4c, d) subsoil configurations and different basement configurations: underground storey (Fig. 4a, c) and embedded floating foundation (Fig. 4b, d). Shear wave velocity profiles are reported on the right-hand side of Fig. 4, with different colours and line types.

Table 1 outlines physical and mechanical properties of soils, masonry and homogeneous material of floor-equivalent beam elements. The shear wave velocity was assigned as mean value of the range related to each category defined by EC8 (CEN 2004), the soil density and the Poisson's ratio were realistically assumed as respectively increasing and decreasing with V_S and representative of gravel (A, B), dense sand (C) and loose sand (D). Mean properties of tuff stone masonry were defined according to experimental results by Augenti and Parisi (2010b). Floor and roof systems were modelled through beam elements with 1 m-wide homogenised cross section, assuming (i) floor systems to be composed of steel I-beams, tiles and poor filling material (i.e. mixed steel-tile systems), and (ii) the pitched roof to be made of timber elements.

4 Discussion of results

4.1 Dynamic analysis of SFS systems

Forty-two plane-strain dynamic analyses in the time domain of SFS models were carried out with the FD code FLAC 2D ver. 7.0 (Itasca 2011). Initial conditions of static

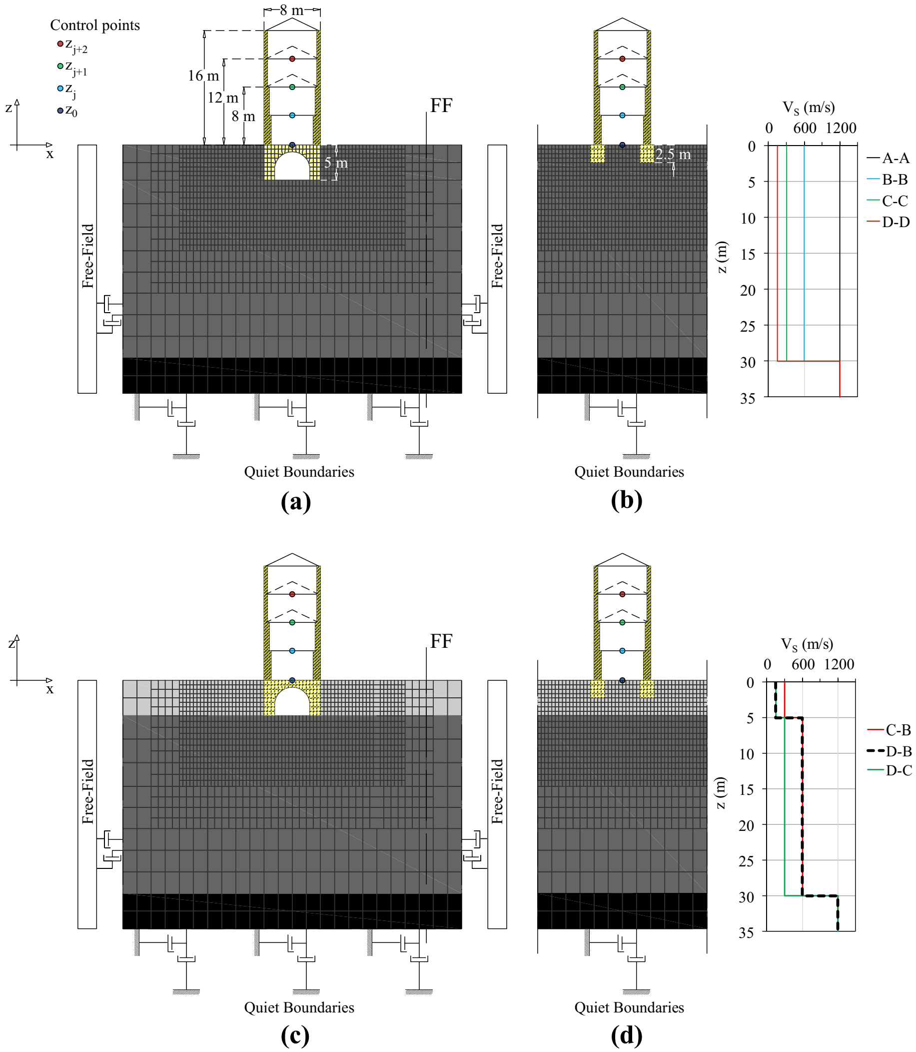

Fig. 4 SFS models of selected case studies with different foundation solutions: **a** homogeneous soil and underground storey; **b** homogeneous soil and embedded floating foundation; **c** layered soil and underground storey; **d** layered soil and embedded floating foundation (shear wave velocity profiles in m/s)

equilibrium under gravity loads were reproduced by simulating the following phases: (1) excavation until the foundation depth; (2) construction of the underground storey/embedded foundations; and (3) construction of the above-ground structure. Since FLAC software is not able to perform modal analysis, the procedure developed by de Silva et al. (2018) was used to compute the fundamental frequency of each SFS system. The SFS model was subjected to a noise signal with duration $t_I = 10$ s (Fig. 5a) and frequency range [1 Hz, 25 Hz] (Fig. 5b), which was applied as a shear stress time-history at the bedrock. The structural response was numerically monitored over 20 s to record the free-vibration behaviour of the SFS system after the end of the forced-vibration stage. Dotted lines in Fig. 5b identify the

Table 1 Physical and mechanical properties of materials

Material	V_S (m/s)	ρ (kg/m^3)	E (MPa)	G (MPa)	ν
Soil type A/Bedrock	1200	2200	7608	3170	0.20
Soil type B	600	2000	1800	720	0.25
Soil type C	300	1800	421	162	0.30
Soil type D	150	1600	97	36	0.35
Tuff stone masonry	–	1600	1080	360	0.49
Homogenised floor material	–	1750	30,000	12,500	0.20
Homogenised roof material	–	300	1300	542	0.20

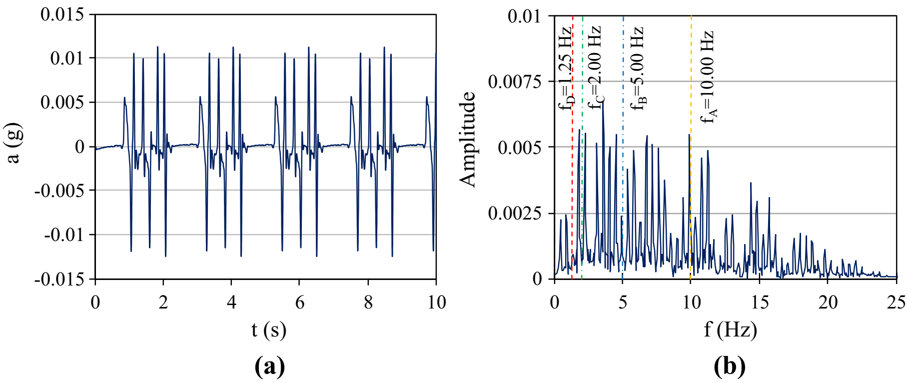

Fig. 5 Input noise for numerical dynamic identification of SFS systems: **a** accelerogram; **b** FFT

fundamental frequencies f_A, f_B, f_C, f_D of homogeneous subsoil volumes associated with the selected code-conforming categories (i.e. A, B, C and D). Such values were evaluated by computing the transfer function as the ratio between the Fast Fourier Transform (FFT) of the free-field acceleration on surface and at bedrock depth along the vertical FF in Fig. 4. The fundamental frequency, f^*, of each SFS system was associated with the peaks of the FFT of the displacement of the control points (Fig. 4) during the free-vibration stage.

Figure 6a and b show the dynamic response of the three-storey structure ($h/b=1.5$) with direct foundation embedded in homogeneous soils A, B, C and D, in terms of displacement time histories at different elevations from $z=0$ to $z=12$ m (see control points in Fig. 4) and FFT computed in the free-vibration stage, respectively. The same results are shown in Fig. 7 for the structure with underground storey. In both cases, f^* is clearly highlighted by spectral peaks, whereas dashed lines indicate the soil fundamental frequencies, denoted as f_{soil}. The comparison between the displacement time histories and FFT during the free oscillation highlights that, moving from soil type A to C, the soil fundamental frequency approaches the frequency of the structure $f_0=2.94$ Hz. Consequently, the peak displacement amplitudes at each elevation gradually increase due to soil-building resonance.

A slight but non-negligible reduction of fundamental frequency of the SFS system under increasing soil deformability is shown by the structure with embedded foundation (Fig. 6) (f^* from 2.94 to 2.70 Hz), whereas the frequency of the structure with underground storey

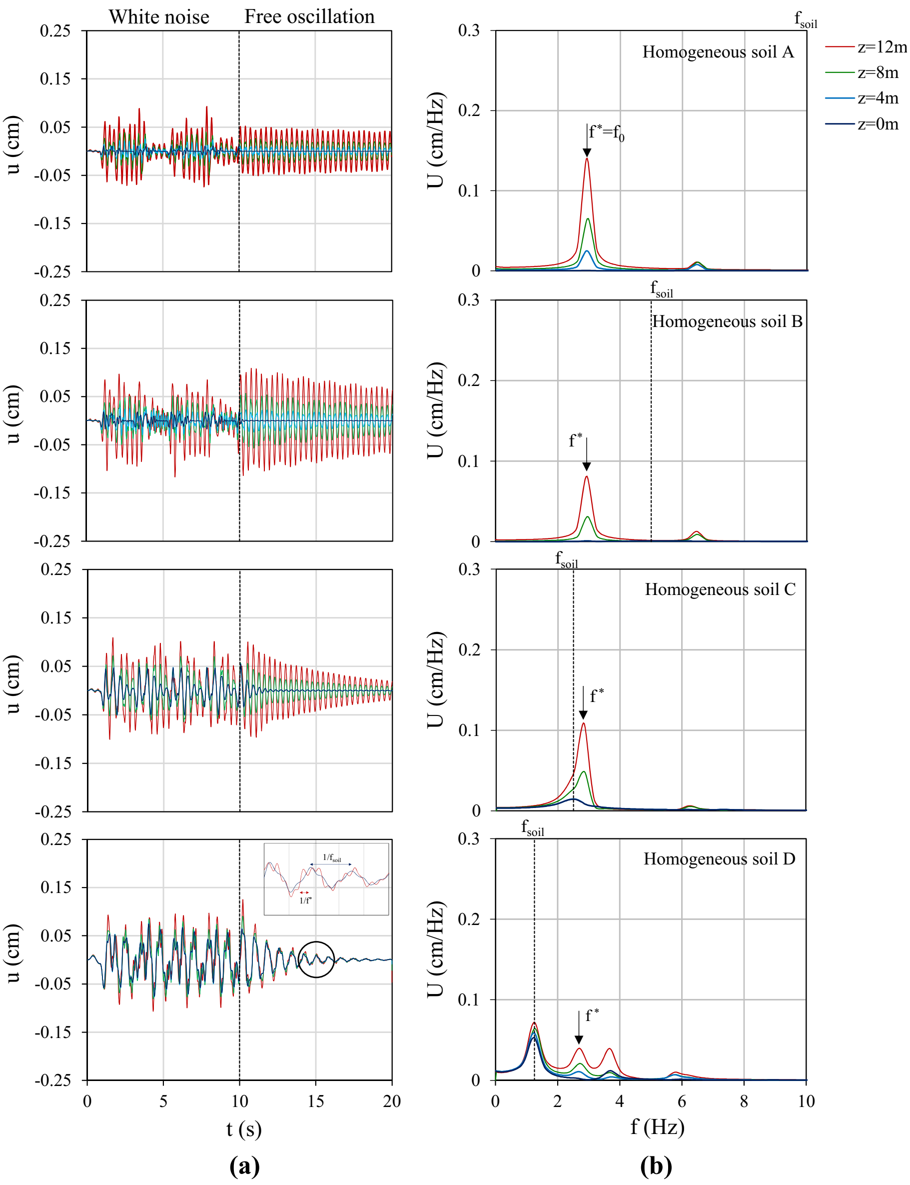

Fig. 6 Dynamic response of three-storey SFS system ($h/b = 1.5$) with embedded floating foundation and homogeneous soil (A, B, C or D): **a** time histories and **b** FFTs of horizontal displacements at different structural elevations

(Fig. 7) was found to be much less affected by the soil type (f^* from 2.94 to 2.82 Hz). In this latter case, the above-ground structure tends to behave as a fixed-base system, due to the massive underground structure. In the case of homogeneous soil D, the FFT highlights two amplitude peaks that are respectively associated with f_{soil} and f^*, confirming that the dynamic behaviour is influenced by soil motion when the relative soil-structure stiffness

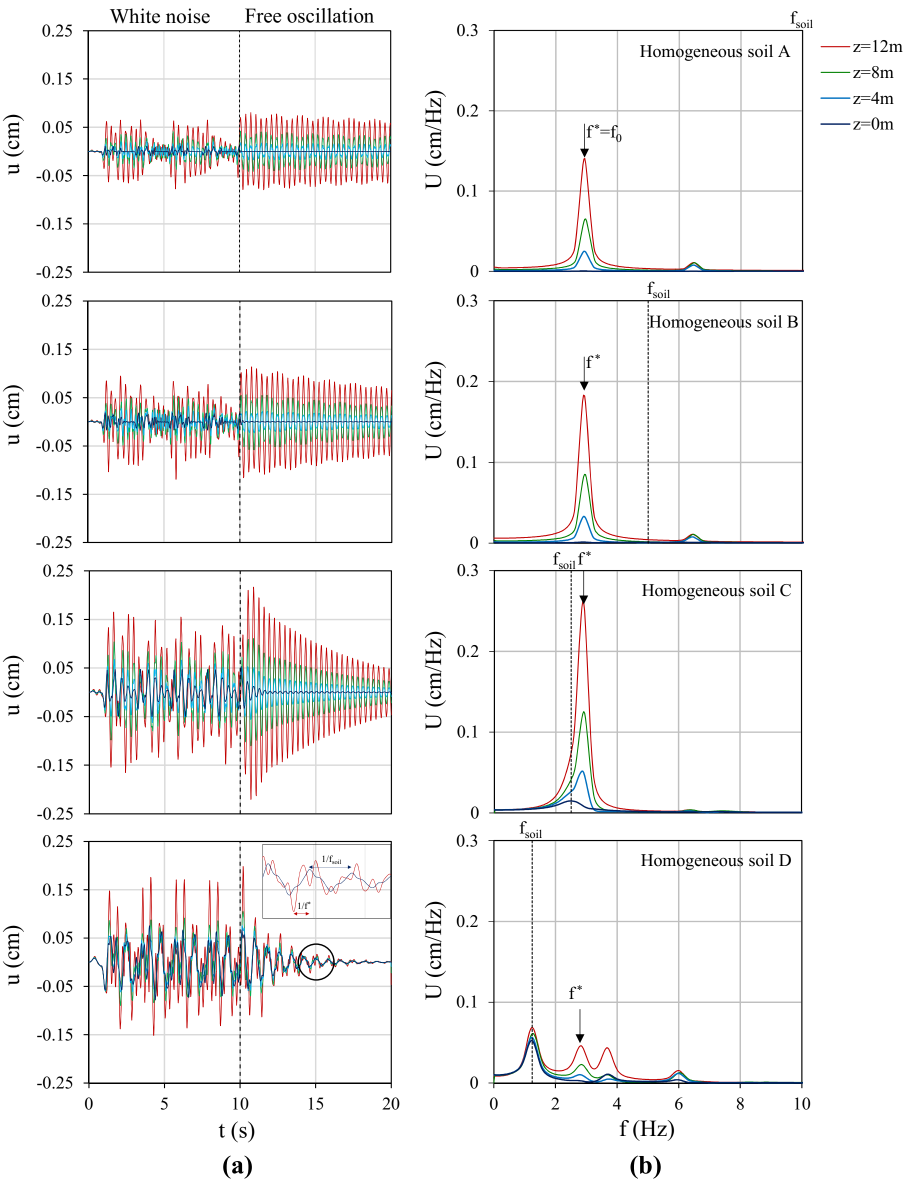

Fig. 7 Dynamic response of three-storey SFS system ($h/b = 1.5$) with underground storey and homogeneous soil (A, B, C or D): **a** time histories and **b** FFTs of horizontal displacements at different structural elevations

is low (de Silva et al. 2019). The enlargements of displacement time histories plotted in the last charts of Figs. 6a and 7a show that horizontal displacements at $z = 12$ m follow the foundation motion with the same frequency.

Tables 2 and 3 provide a summary of fundamental frequencies of the soil and SFS systems with embedded foundation and underground storey, respectively. The fundamental frequency of fixed-base structural systems, which is denoted as f_0, was computed by

Table 2 Fundamental frequencies of soil and SFS systems with embedded foundation ($b/D=3.2$)

Soil configuration	Soil layering	f_{soil} (Hz)	f^* (Hz)		
			$h/b=1$	$h/b=1.5$	$h/b=2$
Homogeneous	A	10.00	**5.01**	**2.94**	**2.02**
	B	5.00	4.92	2.94	2.02
	C	2.50	4.64	2.85	1.97
	D	1.25	3.69	2.70	1.91
Layered	C–B	4.30	4.64	2.85	2.00
	D–B	3.30	4.18	2.73	1.94
	D–C	2.50	4.15	2.64	1.94

Numbers in bold indicate fundamental frequencies of fixed-base systems (i.e. $f^*=f_0$)

Table 3 Fundamental frequencies of soil and SFS systems with underground storey ($b/D=1.6$)

Soil configuration	Soil layering	f_{soil} (Hz)	f^* (Hz)		
			$h/b=1$	$h/b=1.5$	$h/b=2$
Homogeneous	A	10.00	**4.92**	**2.94**	**2.02**
	B	5.00	4.89	2.91	2.02
	C	2.50	4.83	2.88	2.02
	D	1.25	3.69	2.82	2.02
Layered	C–B	4.30	4.83	2.91	2.02
	D–B	3.30	4.70	2.88	2.02
	D–C	2.50	4.64	2.85	1.97

Numbers in bold indicate fundamental frequencies of fixed-base systems (i.e. $f^*=f_0$)

assuming homogeneous soil type A. Numerical results confirm that fixed-base frequencies mainly depend on the aspect ratio of the above-ground structure, rather than the basement system, with appreciable differences only for the squat structure with $h=b$.

As already noted by comparing Figs. 6 and 7, Tables 2 and 3 highlight that the presence of the underground storey causes a lower frequency drop with respect to the case of embedded foundation. As expected, this effect tends to vanish as slenderness increases. For $h>b$ and layered soil configurations, the SFS frequency for both embedded foundation and underground storey approaches the frequency corresponding to the same homogeneous case related to the top layer.

Table 4 allows a comparison between estimates of fundamental frequencies computed in accordance to EC8 (CEN 2004) and those derived from dynamic analysis of fixed-base structural systems.

EC8-conforming estimates of fundamental period, T_{1d}, were obtained as follows:

$$T_{1d} = C_t H^{3/4} \tag{16}$$

where C_t is a structural type coefficient, which was set to 0.05 as provided by EC8 (CEN 2004) in the case of masonry buildings; and H is the overall height (in metres) of the structure computed from the foundation level (i.e. $H=h+D$). Thus, the fundamental frequency

Table 4 Comparison between EC8-conforming and numerical estimates of fundamental frequency

b/D	*h/b*	f_{1d} (Hz)	f_0 (Hz)
3.2	1	3.43	5.01
	1.5	2.70	2.94
	2	2.24	2.02
1.6	1	2.92	4.92
	1.5	2.38	2.94
	2	2.04	2.02

according to EC8 (CEN 2004) was simply defined as $f_{1d}=1/T_{1d}$. Regardless of the ratio b/D, and hence the basement type, Eq. (13) produced an underestimation of the fixed-base fundamental frequency for SFS systems with h/b ranging from 1 to 1.5; the opposite is observed when $h/b=2$. It is also observed that, in the presence of underground storey, the error associated with Eq. (13) tends to vanish because the restraint conditions of the structure become very close to those of a fixed base.

Dynamic analysis of SFS systems under noise signal was also used to evaluate the radiation damping ratio. Figures 6 and 7 show how the decay of peak amplitudes increases with the soil deformability, since a higher amount of energy is dissipated by radiation damping. For each SFS model, the displacement time history was filtered to identify peak amplitudes. Figure 8a shows the filtered (red line) and unfiltered (black line) time histories of the horizontal displacement recorded on top of the three-storey structure ($h/b=1.5$) with underground storey ($b/D=1.6$) embedded in homogeneous soil D.

For each filtered time history, the natural logarithmic amplitude was then computed and plotted against the cycle number, as shown in Fig. 8b. The slope of the linear regression line, i.e. the logarithmic decrement δ, was used to calculate the equivalent damping ratio, ξ^*, as follows:

$$\xi^* = \sqrt{\frac{\delta^2}{4\pi^2 + \delta^2}} \approx \frac{\delta}{2\pi} \tag{17}$$

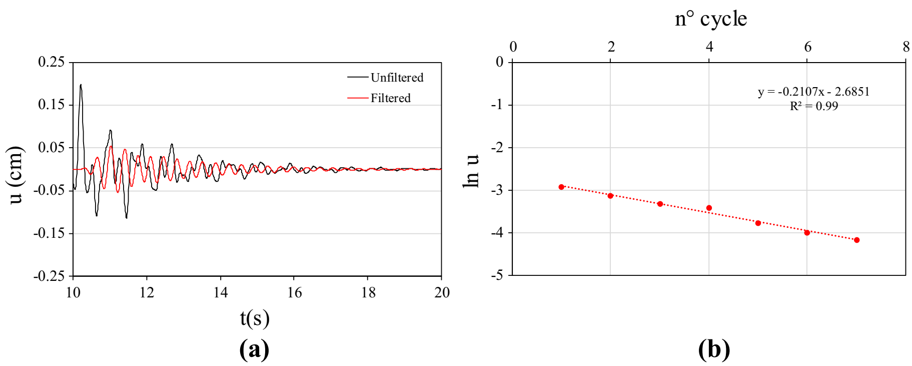

Fig. 8 Computation of radiation damping ratio: **a** unfiltered versus filtered time histories of roof horizontal displacement; **b** logarithmic displacement amplitude versus cycle number

Table 5 Radiation damping ratios of SFS systems with embedded foundation

Soil configuration	Soil layering	ξ_{rad} (%)		
		$h/b = 1$	$h/b = 1.5$	$h/b = 2$
Homogeneous	A	0.24	0.11	0.05
	B	0.99	0.42	0.22
	C	3.36	1.66	1.08
	D	3.79	2.64	2.24
Layered	C–B	1.26	0.53	0.30
	D–B	1.98	0.61	0.38
	D–C	5.44	2.76	1.32

Table 6 Radiation damping ratios of SFS systems with underground storey

Soil configuration	Soil layering	ξ_{rad} (%)		
		$h/b = 1$	$h/b = 1.5$	$h/b = 2$
Homogeneous	A	0.21	0.27	0.26
	B	0.91	0.31	0.27
	C	1.04	1.87	0.77
	D	4.05	3.26	2.56
Layered	C–B	1.40	0.51	0.27
	D–B	1.80	0.44	0.32
	D–C	3.66	3.06	0.94

which turns out to be equal to the radiation damping ratio, given that $\xi_{str} = 0.1\%$ was assigned to the structural model.

Tables 5 and 6 summarize radiation damping ratios related to SFS systems with embedded floating foundation and underground storey, respectively. In most cases, the radiation damping tends to rise up as the soil deformability increases, as shown by the apparently increasing decay of free vibration in Figs. 6a and 7a. Conversely, ξ_{rad} decreases as the slenderness of the structure increases from 1 to 1.5. The presence of the underground storey generally led to higher values of radiation damping because of the larger contact surface between the structure and soil, particularly in homogeneous soil configurations denoted as C and D.

It is worth remembering that very low values of both structural and soil hysteretic damping ratios were assumed, in order to isolate the effect of radiation damping. Since very low strain levels are mobilised in the soil by the low-amplitude input motions adopted in this study, the contribution of the low-strain soil damping can basically be added to the values reported in Tables 5 and 6, as usually done in the application of the RO approach (see Sect. 2.2).

4.2 Application of the replacement oscillator approach

Based on dynamic analysis of SFS systems, a set of replacement oscillators was generated according to the methodology described in Sect. 2.2. For each homogeneous soil configuration, the impedance functions were computed through Eqs. (3) and (4), assuming the shear modulus and Poisson's ratio of the selected soil and accounting for the different embedment of the structure with embedded foundation and underground storey. The fundamental frequency f^* was calculated according to Eq. (6), and the relative soil-structure stiffness parameter σ was evaluated via Eq. (8). This allowed the authors to obtain the data points plotted in Fig. 9a and b for SFS systems with embedded foundation and underground storey, respectively.

In all cases, the foundation length L was set to 1 m in accordance to the procedure used to compute inertia masses and gravity loads. For both the basement configurations, σ was found to range in the intervals [3.75,30], [3.91,34.50] and [4.70,37.50] for structural systems with h/b equal to 1, 1.5 and 2, respectively. For the same aspect ratios, f^*/f_0 was found to range in the following intervals: [0.69,1.00], [0.76,1.00] and [0.84,1.00] in the case of SFS systems with embedded floating foundation; [0.89,1.00], [0.92,1.00] and [0.95,1.00] in the case of SFS systems with underground storey.

Since no direct relationship between σ and f^*/f_0 was defined in the study by Veletsos and Meek (1974), the following function was fitted to each analytical data set related to a given aspect ratio h/b:

$$\frac{f^*}{f_0} = \alpha\sigma^{\beta} + 1 \tag{18}$$

where α and β are regression coefficients, which are listed in Table 7 together with the coefficient of determination R^2. The power law function was constrained to unity at high σ-values, i.e. the fixed-base frequency is obtained for structures on rigid soil. Those curves allow the comparison between analytical predictions and numerical results, as described in Sect. 4.3. It can be noted that, for each basement configuration, a good agreement between analytical data sets and regression models was found.

The analytical solutions of the procedure proposed by Maravas et al. (2014), which is based on Eqs. (10), (11) and (12) in Sect. 2.2, are shown in Fig. 9a and b. If low σ-values are considered, the analytical estimates of the f^*/f_0 ratio according to Maravas et al. (2014) are lower than those calculated in accordance to Veletsos and Meek (1974), producing a slight overestimation of the frequency reduction in the selected case studies. By contrast, the difference between the two sets of analytical solutions becomes negligible at higher σ-values, i.e. when σ is greater than approximately 9.

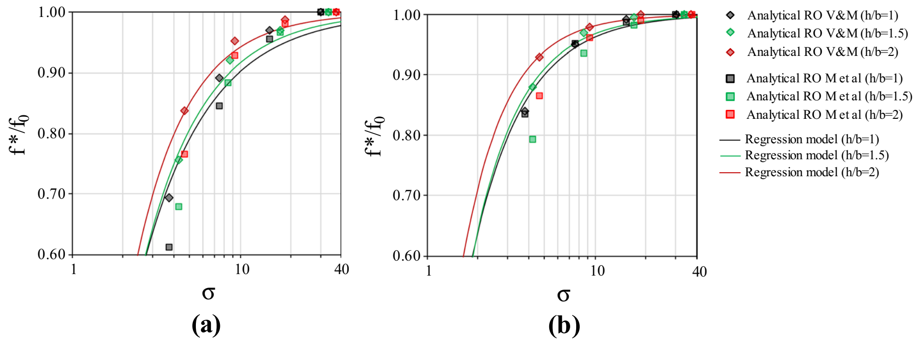

Fig. 9 Regression models for σ-based analytical predictions: **a** structure with embedded floating foundation, **b** structure with underground storey

Table 7 Regression coefficients and coefficient of determination of regression models for estimation of fundamental frequency and radiation damping ratio

b/D	h/b	f			ξ_{rad}		
		α	β	R^2	α	β	R^2
3.2	1	−1.20	−1.09	0.92	60	0.37	1.00
	1.5	−1.33	−1.20	0.99	42	0.39	1.00
	2	−1.37	−1.38	0.99	25	0.38	1.00
1.6	1	−0.95	−1.41	1.00	158	0.47	1.00
	1.5	−1.04	−1.53	1.00	83	0.44	1.00
	2	−0.94	−1.70	0.99	42	0.43	1.00

Nonlinear regression analysis was also carried out on the analytical damping ratios computed by Eq. (7), through the following exponential function:

$$\xi_{rad} = \alpha \exp(-\beta\sigma) \tag{19}$$

Figure 10 shows regression lines together with each set of numerical results up to ξ_{rad} = 20%, which was the graphical upper bound used originally by Veletsos and Meek (1974).

Regression coefficients α and β as well as the coefficient of determination are listed in Table 7. It is noted that regression analysis was carried out over the whole set of data points, that is, without removing data associated with ξ_{rad} > 20%. The procedure proposed by Maravas et al. (2014) was also used to derive analytical estimates of ξ_{rad}, which are compared to regression models in Fig. 10a and b. In all cases, the procedure by Maravas et al. (2014) produced a significant underestimation of ξ_{rad}.

4.3 Comparison between numerical results and analytical predictions

The procedure described in Sect. 4.1 was used to estimate the fundamental frequency and damping ratio of the SFS systems with either embedded foundation or underground storey. Figure 11a and c show the values of f* listed in Tables 1 and 3 normalised to those of the fixed-based systems (first rows in the same tables) and plotted against the soil-structure

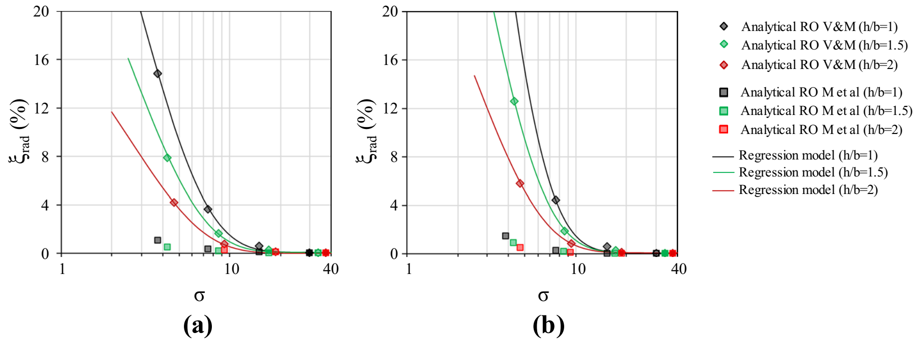

Fig. 10 Regression models for σ-based predictions: **a** structure with embedded foundation, **b** structure with underground storey

stiffness parameter σ corresponding to the shear wave velocity of the in-depth formation, as suggested by Veletsos and Meek (1974).

The regression curves obtained from response predictions of the replacement oscillator described in Sect. 4.2 are shown in Fig. 11. As expected, the fundamental frequency of structures with embedded floating foundation (Fig. 11a) reduces under decreasing σ, and hence the soil stiffness. This effect is confirmed to be practically negligible in the presence of underground storey, except for the models with soil type D (Fig. 11c). In the latter case, the classical calibration of the soil-structure stiffness parameter through the shear wave velocity of the foundation soil can produce an underestimation of SFS interaction effects and the presence of the more deformable lateral soil needs to be taken into account. Dynamic analysis results confirm the analytical trend lines, but are quite scattered, especially for models with layered soil.

Figure 11b highlights how the scatter of numerical data sets obtained for the embedded foundation decreases if σ is replaced by the soil-structure stiffness parameter σ_{eq} defined in Sect. 2.3 and computed from the equivalent shear wave velocity through Eq. (12). The coefficients α_1, α_2 and α_3 into Eqs. (13) and (14) were obtained by minimising the

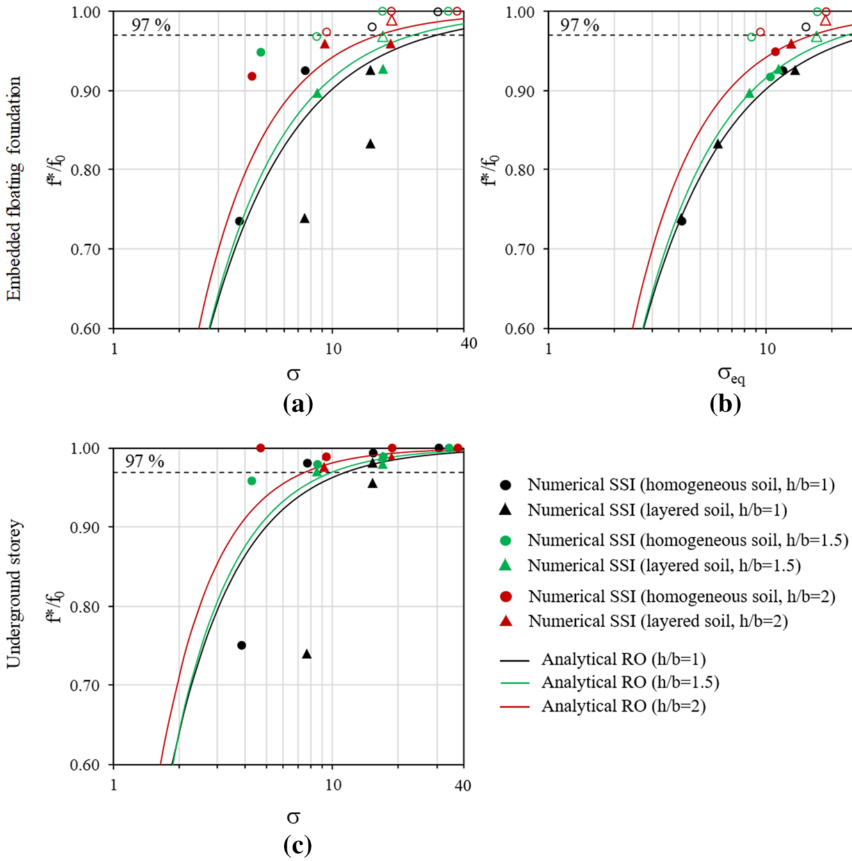

Fig. 11 Comparison between analytical (RO) and numerical (SSI) predictions: **a** structures with embedded foundation and SSI defined through σ; **b** structures with embedded foundation and SSI defined through σ_{eq}; and **c** structures with underground storey

difference between σ_{eq} and the value of σ to be used in Eq. (15) in order to compute the ratio f^*/f_0 given by each numerical analysis. This allowed the authors to reduce the dispersion of numerical results with respect to analytical data. It is also noted that α_1, α_2 and α_3 were calibrated only against analytical solutions of the Veletsos and Meek's formulation. The motivation behind the use of that formulation is twofold: (i) slight differences resulted in the modified frequency with respect to the solution proposed by Maravas et al. (2014); and (ii) the Veletsos and Meek's formulation is widely used in engineering applications. The calibration was performed in numerical cases in which the soil flexibility reduced the frequency ratio f^*/f_0 down to 97%, the latter cut-off level being shown by a dashed, horizontal black line in Fig. 11. Table 8 outlines the calibrated values of coefficients associated with the contribution of shallow cover, in-depth formation and basement system, i.e. α_1, α_2 and α_3 respectively. The estimates of α_1 indicate that the flexibility of the top soil layer significantly influences the dynamic SFS interaction, especially in the case of relatively stiff foundation soil (see, for instance, the output for D-B layering). Indeed, horizontal displacements of the SFS systems are more influenced by the flexibility of lateral soil, rather than that of the in-depth formation, as confirmed by α_2 values mostly close or equal to zero. The latter result is consistent with the low depth of the soil volume affected by the foundation motion reported in the literature.

Furthermore, the effect of foundation stiffness (α_3 values) is predominant for squat structures ($h/b=1$) embedded in soil layering C–C and C-B, as well as for slender structures ($h/b=1.5$ and $h/b=2$) placed on soil softer than masonry (see, for instance, values of E and G in Table 1).

Figure 12 shows the radiation damping ratio computed from numerical results through the procedure described in Sect. 4.1. As the soil stiffness decreases (corresponding to lower values of σ), the energy dissipation capacity of the SFS system increases. In all cases, the numerical estimate of damping ratio (dots in Fig. 12) appears, especially for soil type D, lower than the analytical prediction (solid lines in Fig. 12).

The difference between numerical results and analytical predictions can be mainly ascribed to the fact that the 2D foundation generated in FLAC software (Itasca 2011) neglects the out-of-plane dimension and is made of deformable material. By contrast, a circular rigid plate is assumed in the RO model. Further investigations are necessary to clarify this effect. However, the radiation damping ratio obtained from dynamic analysis under noise input motion rarely exceeds $\xi_{rad}=6\%$, which is a value expected to be significantly exceeded by the hysteretic damping ratio associated with soil nonlinear behaviour under

Table 8 Weighting coefficients for definition of σ_{eq}

h/b	Soil layering	α_1	α_2	α_3
1	C–C	0.00	0.00	1.00
	D–D	1.00	0.04	0.18
	D–B	1.00	0.04	0.00
	D–C	1.00	0.00	0.17
	C–B	0.59	0.80	1.00
1.5	D–D	0.10	0.00	1.00
	D–B	1.00	0.25	0.00
	D–C	0.29	0.39	1.00
2	D–D	0.06	0.03	1.00
	D–B	1.00	0.30	0.00

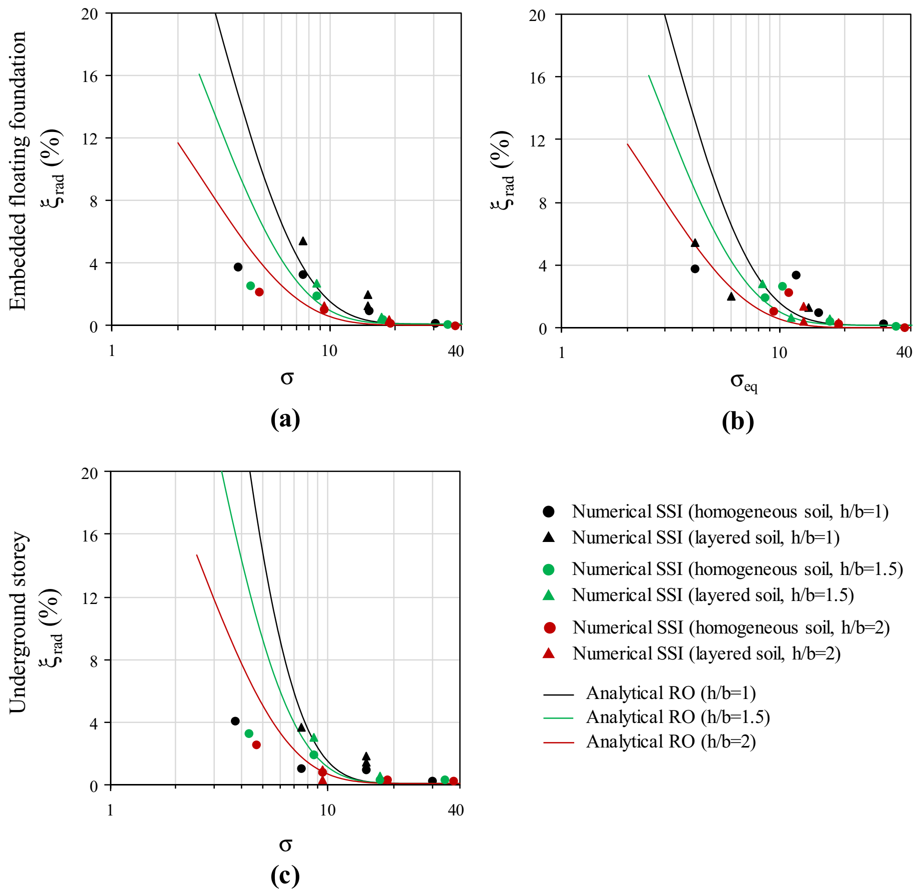

Fig. 12 Comparison between analytical (RO) and numerical (SSI) predictions: **a** structures with embedded foundation and SSI defined through σ; **b** structures with embedded foundation and SSI defined through σ_{eq}; and **c** structures with underground storey

earthquake strong motion. Figure 12b shows the radiation damping ratio plotted against σ_{eq}. Even in this case, if $\sigma_{eq} \leq 10$, the analytical predictions are higher than their numerical counterparts. Conversely, if $\sigma_{eq} > 10$, the RO approach produces rather the same estimates of the numerical models or even an underestimation of ξ_{rad}.

5 Conclusions

This study was aimed at investigating the effects of soil-foundation-structure interaction on the fundamental frequency and radiation damping of 2D SFS models representative of transverse sections of historical masonry buildings, so that out-of-plane loaded walls are included. As the seismic response of the SFS system depends on several geometrical and mechanical properties of the system components, several configurations of above-ground structure (with 2, 3 and 4 storeys), basement (i.e. embedded floating foundation or underground storey) and soil (i.e. homogeneous or layered) were considered, resulting in the generation of forty-two SFS systems. Those configurations, which are typically detected in historical masonry buildings, do not allow the use of simplified formulations available in the literature.

Based on dynamic simulation of SFS systems, the properties of the replacement oscillator (i.e. a flexible-base SDOF system) were calibrated to develop analytical models for quick estimation of fundamental frequency in complex configurations of soil and/or building basement.

The numerical results showed how the dynamic response of the structure is influenced by soil-structure interaction, and how such an interaction depends on soil deformability. SSI effects were found to be attenuated by the presence of an underground storey as well as an increasing height of the structure above ground. The analyses performed on structures founded on layered soil configurations suggest that the fundamental period is mostly affected by the upper soil layer, rather than the stiffer foundation soil. In this respect, to include the contribution by an embedded basement and/or by a layered subsoil, an equivalent soil-structure stiffness parameter has been proposed, significantly improving the analytical predictions of fundamental frequency based on the replacement oscillator approach. Nonetheless, nonlinear regression analysis highlighted that the use of replacement oscillators may produce an overestimation of SSI effects in terms of fundamental frequency reduction and radiation damping increase.

The values of radiation damping ratio provided by coupled SFS systems are not negligible, but significantly lower than closed-form solutions. More significant effects of soil hysteresis and yielding are expected under high strain levels, which are under investigation through nonlinear dynamic analyses of SFS systems under unscaled, real earthquake records.

Given that geometric layouts considered in this study are rather recurrent in the Italian and European building heritage, the proposed procedure might be extensively applied to similar case studies. It is emphasised that a reliable prediction of fundamental frequency and damping accounting for SSI is of critical importance to assess out-of-plane seismic demand on single load-bearing walls of historical masonry buildings, which typically have high vulnerability to local failure modes. Further research is ongoing to assess the effects of masonry type, shallow underground cavities and irregular structural configurations in elevation, as well as to evaluate nonlinear dynamic response under varying seismic input and SFS properties. Additional distinctive aspects of historical masonry buildings include their structural irregularity in plan, as well as the flexibility and geometric complexity of the foundation system.

Acknowledgements This study was carried out within the framework of the 2014-2018 ReLUIS-DPC research project funded by the Italian Civil Protection Department, as part of the geotechnical Work Package 3 ‘Soil-Foundation-Structure Interaction’ and structural Research Line 1 ‘Masonry Structures’.

References

Augenti N, Parisi F (2010a) Learning from construction failures due to the 2009 L’Aquila, Italy, earthquake. J Perform Constr Facil 24(6):536–555

Augenti N, Parisi F (2010b) Constitutive models for tuff masonry under uniaxial compression. J Mater Civ Eng 22(11):1102–1111

Augenti N, Parisi F (2019) Teoria e tecnica delle strutture in muratura. Hoepli, Milan, Italy **(in Italian)**

Augenti N, Parisi F, Prota A, Manfredi G (2011) In-plane lateral response of a full-scale masonry subassemblage with and without an inorganic matrix-grid strengthening system. J Compos Constr 15(4):578–590
Aviles J, Perez-Rocha LE (1996) Evaluation of interaction effects on the system period and the system damping due to foundation embedment and layer depth. Soil Dyn Earthq Eng 15:11–27
Aviles J, Perez-Rocha LE (1998) Effects of foundation embedment during building-soil interaction. Earthq Eng Struct Dyn 27:1523–1540
Beredugo YO, Novak M (1972) Coupled horizontal and rocking vibration of embedded footings. Can Geotech J 9(4):477–497
Bielak J (1975) Dynamic behavior of structures with embedded foundation. Earthq Eng Struct Dyn 3:259–274
Bruneau M (1994) State-of-the-art report on seismic performance of unreinforced masonry buildings. J Struct Eng 120(1):230–251
Casciati S, Borja RI (2004) Dynamic FE analysis of south memnon colossus including 3D soil-foundation-structure interaction. Comput Struct 82:1719–1736
Cattari S, Sivori D, Brunelli A, Sica S, Piro A, de Silva F, Parisi F, Silvestri F (2019) Soil-structure interaction effects on the dynamic behavior of a masonry school damaged by the 2016–2017 Central Italy earthquake sequence. In: Proceedings of 7th International Conference on Earthquake Geotechnical Engineering, Rome, 17–20 June 2019
CEN (2004) Eurocode 8: design of structures for earthquake resistance—part 1: general rules, seismic actions and rules for buildings. EN 1998-1:2004, Comité Européen de Normalisation, Brussels
Ceroni F, Sica S, Pecce MR, Garofano A (2014) Evaluation of the natural vibration frequencies of a historical masonry building accounting for SSI. Soil Dyn Earthq Eng 64:95–101
Conti R, Morigi M, Viggiani MB (2016) Filtering effect induced by rigid massless embedded foundations. Bull Earthq Eng 15:1019–1035
Cosentini RM, Foti S, Lancellotta R, Sabia D (2015) Dynamic behavior of shallow founded historic towers: validation of simplified approaches for seismic analyses. Int J Geotech Eng 9(1):13–29
D'Ayala DF, Paganoni S (2011) Assessment and analysis of damage in L'Aquila historic city centre after 6th April 2009. Bull Earthq Eng 9(1):81–104
de Silva F, Sica S, Silvestri F, Aversa S (2016) Estimation of the ground shaking from the response of rigid bodies. Annals of Geophysics, 59, Fast Track 5 of the special issue: The Amatrice seismic sequence: preliminary data and results, 2016; https://doi.org/10.4401/ag-7296
de Silva F, Pitilakis D, Ceroni F, Sica S, Silvestri F (2018) Experimental and numerical dynamic identification of Carmine bell tower in Naples (Italy). Soil Dyn Earthq Eng 109:235–250
de Silva F, Ceroni F, Sica S, Silvestri F (2019) Fragility curves of slender towers accounting for soil-structure interaction. In: Proceedings of 7th International Conference on Earthquake Geotechnical Engineering, Rome, 17–20 June 2019
Dominguez J (1978) Dynamic stiffness of rectangular foundations. Research Report R78-20. Department of Civil Engineering, Massachusetts Institute of Technology, Cambridge
Elsabee F, Morray JP (1977) Dynamic behavior of embedded foundations. Research Report R77-33, Massachusetts Institute of Technology, Cambridge
Faccioli E, Paolucci R, Vanini M (1998) 3D site effects and soil-foundation interaction in earthquake and vibration risk evaluation. Final report of the European research project TRISEE. European Commission, Brussels
Gazetas G (1983) Analysis of machine foundation vibrations: state of the art. Soil Dyn Earthq Eng 2:1–41
Gazetas G (1991) Formulas and charts for impedances of surface and embedded foundations. J Geotech Eng 117:1363–1381
Gazetas G (2015) 4th Ishihara lecture: soil-foundation-structure systems beyond conventional seismic failure thresholds. Soil Dyn Earthq Eng 68:23–39
Gerolymos N, Gazetas G (2006a) Winkler model for lateral response of rigid caisson foundations in linear soil. Soil Dyn Earthq Eng 26(5):347–361
Gerolymos N, Gazetas G (2006b) Development of Winkler model for static and dynamic response of caisson foundations with soil and interface nonlinearities. Soil Dyn Earthq Eng 26(5):363–376
Gerolymos N, Gazetas G (2006c) Static and dynamic response of massive caisson foundations with soil and interface nonlinearities—validation and results. Soil Dyn Earthq Eng 26(5):377–394
Givens MJ, Mylonakis G, Stewart JP (2016) Modular analytical solutions for foundation damping in soil-structure interaction applications. Earthq Spectra 32(3):1749–1768
Guerrini G, Graziotti F, Penna A, Magenes G (2017) Improved evaluation of inelastic displacement demands for short period masonry structures. Earthq Eng Struct Dyn 46:1411–1430

Itasca (2011) FLAC 7.0—fast lagrangian analysis of continua—user's guide, Itasca Consulting Group, Minneapolis
Jahankhah H, Farashahi PF (2017) The effect of foundation embedment on net horizontal foundation input motion: the case of strip foundation with incomplete contact to nearby medium. Soil Dyn Earthq Eng 96:35–48
Jaya KP, Meher Prasad A (2002) Embedded foundation in layered soil under dynamic excitations. Soil Dyn Earthq Eng 22:485–498
Kallioras S, Guerrini G, Tomassetti U, Marchesi B, Penna A, Graziotti F, Magenes G (2018) Experimental seismic performance of a full-scale unreinforced clay-masonry building with flexible timber diaphragms. Eng Struct 161:231–249
Karapiperis K, Gerolymos N (2014) Combined loading of caisson foundations in cohesive soil: finite element versus Winkler modeling. Comput Geotech 56:100–120
Kausel E (2010) Early history of soil-structure interaction. Soil Dyn Earthq Eng 30:822–832
Kausel E, Roesset JM (1975) Dynamic stiffness of circular foundations. J Eng Mech Div 101(6):770–785
Kim S, Stewart JP (2003) Kinematic soil-structure interaction from strong motion recordings. J Geotech Geoenviron Eng 129:323–335
Kuhlemeyer RL, Lysmer J (1973) Finite element method accuracy for wave propagation problems. J Soil Mech Found Div 99(SM5):421–427
Lagomarsino S, Cattari S (2015) PERPETUATE guidelines for seismic performance based assessment of cultural heritage masonry structures. Bull Earthq Eng 13(1):13–47
Lourenço PB (1996) Computational strategies for masonry structures. PhD Thesis, Delft University of Technology, Delft, The Netherlands
Madiai C, Renzi S, Vannucchi G (2013) Seismic risk assessment of San Gimignano towers: Geotechnical aspects and soil-structure interaction. Geotechnology engineering for the preservation of monuments and historic sites. Taylor & Francis Group, London, pp 523–530
Maravas A, Mylonakis G, Karabalis LD (2014) Simplified discrete systems for dynamic analysis of structures on footings and piles. Soil Dyn Earthq Eng 61–62:29–39
Meek W, Wolf JP (1994) Cone models for embedded foundation. J Geotech Eng 120:60–80
MIT (2018) Norme Tecniche per le Costruzioni. DM 17/1/2018, Italian Ministry of Infrastructure and Transportation, Rome, Italy **(in Italian)**
Mylonakis G, Gazetas G (2000) Seismic soil-structure interaction: beneficial or detrimental. J Earthq Eng 4:277–301
Mylonakis G, Nikolaou S, Gazetas G (2006) Footings under seismic loading: analysis and design issues with emphasis on bridge foundations. Soil Dyn Earthq Eng 26:824–853
Parisi F, Augenti N, Prota A (2014) Implications of the spandrel type on the lateral behavior of unreinforced masonry walls. Earthq Eng Struct Dyn 43(12):1867–1887
Parisi F, Balestrieri C, Varum H (2019) Nonlinear finite element model for traditional adobe masonry. Constr Build Mater 223:450–462
Penna A, Morandi P, Rota M, Manzini CF, da Porto F, Magenes G (2014) Performance of masonry buildings during the Emilia 2012 earthquake. Bull Earthq Eng 12(5):2255–2273
Piro A, de Silva F, Scotto di Santolo A, Parisi F, Silvestri F (2018) Sensitivity analysis of seismic soil-cavity-structure interaction in historic urban centres. In: Proceedings of 16th European conference earthquake engineering, Thessaloniki, 18–21 June 2018
Pitilakis D, Karatzetzou A (2015) Dynamic stiffness of monumental flexible masonry foundations. Bull Earthq Eng 13:67–82
Shirato M, Kuono T, Asai R, Fukui J, Paolucci R (2008) Large scale experiments on nonlinear behavior of shallow foundations subjected to strong earthquakes. Soils Found 48:673–692
Sorrentino L, Liberatore L, Liberatore D, Masiani R (2014) The behaviour of vernacular buildings in the 2012 Emilia earthquakes. Bull Earthq Eng 12(5):2367–2382
Spyrakos CC, Beskos D (1986) Dynamic response of flexible strip foundation by boundary and finite elements. Soil Dyn Earthq Eng 5(2):84–96
Stewart JP, Fenves G, Seed R (1999) Seismic soil-structure interaction in buildings. I: analytical methods. J Geotech Geoenviron Eng 125:26–37
Stewart JP, Kim S, Bielak J, Dobry R, Power M (2003) Revisions to soil-structure interaction procedures in NEHRP design provisions. Earthq Spectra 19(3):677–696
Tomaževič M, Weiss P (2010) Displacement capacity of masonry buildings as a basis for the assessment of behavior factor: an experimental study. Bull Earthq Eng 8(6):1267–1294
Varun V, Assimaki D, Gazetas G (2009) A simplified model for lateral response of large diameter caisson foundations—Linear elastic formulation. Soil Dyn Earthq Eng 29(2):268–291

Veletsos A, Meek JW (1974) Dynamic behavior of building-foundation systems. Earthq Eng Struct Dyn 3:121–138

Veletsos AS, Nair VV (1975) Seismic interaction of structures on hysteretic foundation. J Struct Eng 101:109–129

Vuoto A, Piro A, de Silva F, Scotto di Santolo A, Parisi F, Silvestri F (2018) Seismic soil-structure interaction: two case studies in Sant'Agata de' Goti, Italy. In: Proceedings of 16th European conference earthquake engineering, Thessaloniki, 18–21 June 2018

Wolf J (1985) Dynamic soil-structure interaction. Prentice Hall, Englewood Cliff

Affiliations

Annachiara Piro[1] · Filomena de Silva[2] · Fulvio Parisi[1] · Anna Scotto di Santolo[3] · Francesco Silvestri[2]

Filomena de Silva
filomena.desilva@unina.it

Fulvio Parisi
fulvio.parisi@unina.it

Anna Scotto di Santolo
anna.scottodisantolo@unipegaso.it

Francesco Silvestri
francesco.silvestri@unina.it

[1] Department of Structures for Engineering and Architecture, University of Naples Federico II, Naples, Italy

[2] Department of Civil, Architectural and Environmental Engineering, University of Naples Federico II, Naples, Italy

[3] Telematic University Pegaso, Naples, Italy